Molecular insights into the self-assembly mechanism of dystrophia myotonica kinase

Pilar Garcia,* Zöhre Ucurum,* Rainer Bucher,* Dmitri I. Svergun,† Thomas Huber,‡ Ariel Lustig,* Petr V. Konarev,† Marco Marino,* Olga Mayans*,[1]

*Division of Structural Biology, Biozentrum, University of Basel, Basel, Switzerland; †European Molecular Biology Laboratory, Hamburg Outstation, c/o DESY, Hamburg, Germany and Institute of Crystallography, Russian Academy of Sciences, Moscow, Russia; and ‡Biochemisches Institut, Universität Zürich, Zürich, Switzerland

ABSTRACT **Self-assembly via coiled-coil domains (CC) is crucial for the regulation of the dystrophia myotonica kinase (DMPK) -related family of kinases. These CC domains are thought to form dimeric arrangements and thus to mediate dimerization in these enzymes. Using size exclusion chromatography combined with multiangle static light scattering, we analyzed the oligomeric state of DMPK as well as that of a truncated variant lacking the CC fraction. Remarkably, both forms were found to assemble into robust dimers. In contrast, the CC domain in isolation yielded trimeric assemblies, indicating that the oligomerization properties of CC domains from this kinase family are more diversified than anticipated. The crystal structure of this CC has been elucidated to 1.6 Å resolution and its properties in solution established using sedimentation equilibrium and thermal denaturation. These data show that, contrary to expectations, the self-assembly of DMPK is not dictated by the association properties of its CC domain. Instead, it appears to be driven by sequence segments flanking both N and C termini of the catalytic kinase fraction, as suggested by models of head-to-head dimers based on small angle X-ray scattering data. Our findings support a shared pattern of assembly across DMPK, ROCKs, and MRCK members of this family.—Garcia, P., Ucurum, Z., Bucher, R., Svergun, D. I., Huber, T., Lustig, A., Konarev, P. V., Marino, M., Mayans, O. Molecular insights into the self-assembly mechanism of dystrophia myotonica kinase. *FASEB J.* 20, 1142–1151 (2006)**

Key Words: kinase · coiled-coil · protein assembly · protein structure · X-ray crystallography · multiangle static light scattering · small angle X-ray scattering

Self-assembly is a main feature of the dystrophia myotonica kinase (DMPK) -related family of kinases. These complex multidomain kinases share a highly conserved catalytic domain and a coiled-coil fraction (CC) involved in the regulation of their activity. To this group belong DMPK (1, 2), Rho-associated kinases I and II (ROCKI/ II, also known as β and α, respectively) (3, 4), *C. elegans* LET-502 (5), *Drosophila* Genghis Khan kinase (Gek) (6), murine citron kinase (7), and rat Cdc42 binding kinase (MRCK) (8), among others. Most of these kinases act as effectors of small Rho GTPases (Rho, Rac, and Cdc42 subclasses) known to regulate cytoskeletal dynamics. Accordingly, several members of the family are functionally linked to cytoskeletal reorganization events, as illustrated by the involvement of Gek in actin polymerization (6) and the role of citron kinase, LET-502, and ROCKII in regulating the cleavage furrow contraction during cytokinesis (9–11).

DMPK is regarded as the defining member of this kinase family. It is most closely related to MRCK and ROCKs, with which it shares sequence similarity across the N-terminal catalytic fraction but not across CC moieties (**Fig. 1**). By analogy to other family members, DMPK is suspected to regulate cytoskeletal events (12, 13) and may act as a downstream effector in the regulatory pathways of RhoA (12) and Rac1 (14). Other reports, however, defend that DMPK intervenes in the modulation of the electrical excitability of the plasma membrane (15, 16). Taken together, functional data suggest that DMPK might be related to muscle stiffness and hyperexcitability, heart conduction defects, and cognitive deficit in a progressive neuromuscular disorder known as myotonic dystrophy (DM1), which is the most common form of muscular dystrophy in adults (17). DM1 patients suffer from DMPK insufficiency due to the retention of mRNA transcripts in the nucleus (18, 19). However, it is not currently understood how low levels of this kinase affect cellular function, and thus its involvement in disease remains polemic.

Oligomerization via CC segments is thought to be central to the regulation of DMPK-related kinases. CC motifs consist of two to five amphipathic α-helices that wind around each other to form, typically, a left-handed supercoil. They mediate self-assembly events in proteins but can also be implicated in refolding processes and molecular recognition (for a recent review, see ref 20). CC sequences are characterized by a repeat

[1] Correspondence: Division of Structural Biology, Biozentrum, University of Basel, Klingelbergstr. 70, Basel CH-4056, Switzerland. E-mail: olga.mayans@unibas.ch

doi: 10.1096/fj.05-5262com

0892-6638/06/0020-1142 © FASEB

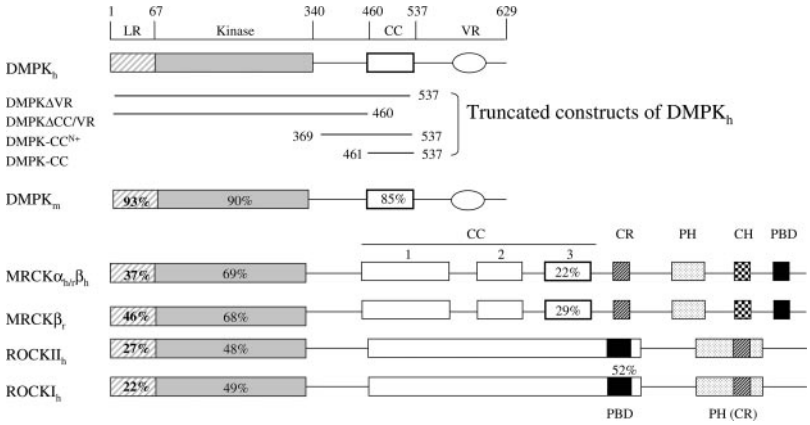

Figure 1. Domain organization in DMPK, MRCK, and ROCK. Domain composition of human DMPK (Q09013–9), mouse DMPK (P54265), human MRCKα (Q5VT26), rat MRCKα (AF021935), human MRCKβ (Q81WQ7), mouse ROCKII (V58513), and mouse ROCKI (V58512). LR: leucine-rich region; CC: coiled-coil; VR: region variable across DMPK spliceoforms. CR: cysteine-rich domain, PH: pleckstrin homology domain; CH: citron homology domain; PBD: p21 GTPase binding domain. Sequence identity to human DMPK is given as percentage where applicable. DMPK constructs used in the current study are shown.

pattern of seven amino acids denoted *a* to *g*. Positions *a* and *d* classically harbor hydrophobic residues, which constitute the structural core of the motif. Positions *e* and *g* often host charged groups that form networks of intra- and interhelical salt bridges crucial to fold stability and interchain recognition. CC domains from DMPK-related kinases are believed to form dimeric assemblies and thereby to mediate dimerization in these enzymes. To date, only two closely related CC fragments from this family have been characterized. These correspond to the C-terminal, Rho binding motifs of ROCKII-CC and ROCKI-CC that share 52% sequence identity (Fig. 1). For these, crystal structures have been reported in free form (21) and complexed to RhoA (22), respectively, confirming that both coils form parallel dimers. In a similar way, only a few analytical studies have reported on the oligomerization state of full-length kinases. Currently, data are available only for DMPK (23) and ROCKs (24, 25), which have been shown to adopt dimeric states. Despite the similarity of these kinases, different mechanisms have been proposed for their dimerization. While data on DMPK defended a self-assembly driven by its CC motif (23), the reports on ROCKs prove that CC moieties are not required for their oligomerization. The latter agrees with a biochemical study of MRCK, which also reported self-association in the absence of CC fractions (26). The associative interactions in ROCKs are the best understood so far due to the recent availability of the crystal structure from the dimeric N-terminal fraction (i.e., lacking CC segments) from ROCKI (25). This shows how head-to-head dimers interact via a small, N-terminal domain comprising the α-helical LR region (Fig. 1) as well as a tail, C-terminal to the kinase domain, which wraps around the catalytic core to reach the subunit interface. Given that dimerization segments show a certain homology across DMPK, ROCKs, and MRCK (Fig. 1), it would be reasonable to expect that related mechanism of assembly could be supported by these kinases, even if conflicting data have been reported (23).

Moreover, different biochemical roles have been attributed to the CC moieties of these kinases. The CC domains of ROCKs and citron kinase act as intrasteric inhibitors of their respective kinase domains and house at their C termini binding motifs for small Rho GTPases, where binding of the latter releases the inhibition (7, 27). CC segments of MRCK (CC2/CC3) also act as intrasteric inhibitors but do not host a GTPase binding region (26), and physiological release factors are yet to be identified. On the contrary, the CC fraction of DMPK (DMPK-CC) has been proposed to act as an enhancer of its kinase activity (23), although it is unknown whether this involves transphosphorylation events as those observed in tyrosine kinases. In summary, both the functionality of CC domains from this family and the extent to which they govern molecular assembly remain unclear. Given that the CC from DMPK appears to differ from those of ROCKs and MRCK both in its regulatory properties and in its role during assembly (23), we have investigated the architectural details of DMPK to assess whether a common association principle exists in this family of kinases.

MATERIALS AND METHODS

Cloning

Expression constructs were derived from human DMPK cDNA (L08835) spanning residue ranges as shown in Fig 1. DMPKΔVR was cloned into the *Eco*RI and *Sal*I sites of the insect cell expression vector pFastBac1 (Invitrogen, San Diego, CA, USA). A His_6-tag and a TEV (tobacco etch virus) protease cleavage site were inserted N-terminal to the target construct. DMPKΔCC/VR was cloned into pET-15b (Novagen, Madison, WI, USA) using primers 5′-GGAATTCCATATGTCAGCCGAGGTGCG-3′ and 5′-CGGGATCCTTACCCCGTGACAGCTGTGG-3′ with *Nde*I and *Bam*HI restriction sites, respectively. This vector adds a His_6-tag and a thrombin cleavage site N-terminal to the target protein. Cloning of DMPK-CC has been previously reported (28). DMPK-CC^{N+} was cloned into the pETM-11 vector, a modified version of pET-24d (Novagen) that includes a His_6-tag plus a TEV protease cleavage site N-terminal to the expression construct. This used primers 5′-CGTTCGAAGACTACATGTTGGTGGAGGACGGGCTC-3′ and 5′-GGGGTACCTTACCCCGTGACAGCTGTGG-3′ carrying BbsI (*Nco*I-compatible) and *Kpn*I restriction sites.

Protein production

Sf9 cells were transfected with the bacmic cDNA construct of DMPKΔVR according to the manufacturer's instructions

(Life Technologies Bac-to-Bac system). The transfected cells were incubated for 3 days at 27°C and the supernatant, containing recombinant virus for protein expression, was collected. Amplified virus (10 ml) was added to 1×10^6 Sf9 cells and incubated at 27°C for 3 days. Lysis was performed by incubation on ice for 30 min in the presence of DNase and protease inhibitors (Complete EDTA-free; Roche, Nutley, NJ, USA) in 50 mM Tris pH 8.0, 300 mM NaCl, 5 mM β-mercaptoethanol, 2% glycerol. A clarified supernatant was obtained by centrifugation at 20,000 rpm and 4°C for 1 h. The protein product was purified by affinity chromatography on a His-Trap HP column (GE Healthcare) equilibrated in lysis media. The bound protein was eluted by supplementing the medium with 200 mM imidazole. Subsequent purification used size exclusion chromatography on a Superdex 200 Tricorn 10/30 GL column (GE Healthcare) in 50 mM Tris pH 8.0, 150 mM NaCl, 5 mM β-mercaptoethanol, 2% glycerol.

DMPKΔCC/VR was expressed in *E. coli* Rosetta (DE3) (Novagen) grown in LB medium supplemented with 34 μg/ml of chloramphenicol and 100 μg/ml ampicillin. Induction used 1 mM IPTG and incubation was overnight at 25°C. Cells were harvested by centrifugation at 8000 *g* at 4°C for 15 min. Lysis was by French pressing in the presence of DNase and protease inhibitors in 50 mM Tris pH 8.0, 50 mM NaCl, 5 mM β-mercaptoethanol. The clarified supernatant, obtained by centrifugation at 20,000 rpm (4°C), was purified by affinity chromatography and subsequent gel filtration (as described for DMPKΔVR) in lysis media. Expression and purification of DMPK-CC were as reported (28). Production of DMPK-CC^{N+} used protocols as for DMPK-CC, except that all media were supplemented with 5 mM β-mercaptoethanol. All measurements used fresh preparations and sample identification was by peptide-digest mass spectrometry.

Structure determination

Crystallization, data collection, data statistics, and experimental phasing of DMPK-CC have been described (28). Briefly, crystals grew from 100 mM Tris-HCl pH 7.5, 2.0 M Na^+/K^+ tartrate and 5–10 mg/ml protein solutions. X-ray diffraction data collected at beamline ID14–2 (ESRF, Grenoble) revealed the crystals to belong to space group $P2_12_12_1$ with unit cell dimensions of a = 39.1 Å, b = 46.2 Å, c = 143.5 Å, and three polypeptide chains per asymmetric unit. Experimental phasing used 3λ MAD on an Se-Met derivative. Phase refinement was in SHARP (29) and automatic model improvement in ARP/warp v6.1 (30). Manual model building used the software O (31) and refinement was in REFMAC (32). For cross-validation, crystallographic data were divided into a working and a test set using FREERFLAG (33). Restraints for non-crystallographic symmetry were applied during the initial phase of refinement and released at later stages. Geometrical parameters of intermediate and final models were assessed using PROCHECK (34). The final model lacks several N- and C-terminal residues that could not be resolved in electron density maps, namely 461–465/530–537 in chain A, 461–463/528–537 in chain B and 461–465/527–537 in chain C. This amounts to ~20% of disorder in the structure and explains the slightly elevated R-factor values, which are somewhat above those characteristic of this resolution. Coordinates have been deposited at the Protein Data Bank with accession number 1WT6.

Analytical ultracentrifugation

Sedimentation velocity and equilibrium data were recorded using an Optima XL-A analytical ultracentrifuge (Beckman Instruments, Fullerton, CA, USA) equipped with 4 and 12-mm Epon double-sector cells in an An-60 Ti rotor and absorption optics. Runs were performed at 20°C in *1)* 50 mM Tris pH 7.5, 50 mM NaCl and *2)* 100 mM sodium phosphate pH 7.0 using detection wavelengths of 277 nm and 234 nm. Sedimentation velocity experiments were carried out at 54,000 rpm and 0.65 mg/ml sample concentration. Sedimentation equilibrium measurements were performed at 19,000, 21,000, 24,000, and 26,000 rpm, and protein concentrations of 0.16–3.3 mg/ml for DMPK-CC and 0.09–1.4 mg/ml for DMPK-CC^{N+}, where optical density values remained in a linear range. Average molecular masses were evaluated using SEGAL (G. Machaidze and A. Lustig, unpublished software), which adjusts the baseline absorbance to obtain the best linear fit of ln(absorbance) vs. radial distance square. A protein partial specific volume of 0.73 ml/g was used, while solution density was taken as 1.003 g/ml and viscosity as 1.02 centipoise.

Circular dichroism spectroscopy

Thermal denaturation of DMPK-CC was monitored at 222 nM on a 62A DS circular dichroism spectropolarimeter (AVIV) equipped with a temperature-controlled quartz cell of 2 mm optical path over a temperature range of 5–90°C. The scan speed was 0.5°C/min with a spectral bandwidth of 2.0 nm.

Binding assays

The binding of DMPK-CC to DMPKΔCC/VR was assayed in 50 mM Tris-HCl pH 7.5, 100 mM NaCl by *1)* affinity pull-down assays using His_6-tagged DMPKΔCC/VR immobilized in a His-Trap HP column (GE Healthcare) vs. a flow of untagged DMPK-CC; *2)* simultaneous coexpression of both constructs followed by attempts of copurification via metal affinity plus size exclusion chromatography (protocols as above).

Size exclusion chromatography combined with multiangle light scattering (SEC-MALS)

The oligomeric state of DMPKΔVR and DMPKΔCC/VR in solution was determined via SECMALS measurements performed on an ÅKTA explorer 10 system (GE Healthcare) connected to a triangle light scattering detector and a differential refractometer (miniDAWN Tristar and Optilab, respectively; Wyatt Technology, Santa Barbara, CA, USA). A Superdex 200 HR 10/30 column (GE Healthcare) was used in 50 mM Tris-HCl pH 8.0, 50 mM NaCl at a flow rate of 0.5 ml/min. Sample volumes of 50 μl (DMPKΔVR) and 100 μl (DMPKΔCC/VR) were injected at a concentration of 2 mg/ml. A specific refractive index increment (dn/dc) value of 0.185 ml/g was used. The data were recorded and processed using ASTRA software (Wyatt Technology). To determine the detector delay volumes and normalization coefficients for the MALS detector, a BSA sample (Sigma A-8531) was used as reference. Neither despiking nor band broadening correction was applied.

Small angle X-ray scattering (SAXS)

Synchrotron radiation SAXS data were collected on the X33 camera (35) of EMBL (DESY, Hamburg). Solutions of DMPKΔCC/VR were measured at protein concentrations of 1.4, 3.8, 5.7, 8.5, and 9.3 mg/ml in 50 mM TrisHCl pH 8.0, 50 mM NaCl, 2.5 mM β-mercaptoethanol at 4°C. Measurements were recorded using a MAR345 IP detector at a sample detector distance of 2.7 m and wavelength λ = 1.5 Å in the range of momentum transfer $0.011 < s < 0.45$ $Å^{-1}$. Exposure time for a single measurement was 5 min. To check for

TABLE 1. *X-ray data statistics and model parameters*

X-ray data	
Space group	$P2_12_12_1$
Resolution (Å)	20–1.6 (1.69–1.6)
Unique reflections	33876 (3951)
Completeness (%)	96.3 (79.2)
$R_{sym}(I)$	0.059 (0.330)
Multiplicity	4.4 (2.3)
$<I/\sigma(I)>$	15.0 (2.5)
Model refinement	
Resolution (Å)	20–1.6
Reflections working/free	32044/1712
R-factor/R-free (%)	22.7/27.0
Chains per asymmetric unit	3
No. protein/solvent atoms	1619/294
Average B ($Å^2$)	26.05
Rmsd bond lengths (Å)/ angles (°)	0.019/1.717
Residues in Ramachandran core / disallowed (%)	99.5/0

radiation damage, two consecutive 3 min exposures at the highest protein concentration were compared and no changes were observed. The data were normalized, the scattering of the buffer subtracted, and the difference curves extrapolated to zero solute concentration using the program package PRIMUS (36). The maximum particle dimension D_{max}, forward scattering I (0) and the radius of gyration R_g were evaluated using GNOM (37). The molecular mass (MM) of the solute was calculated by comparing its forward scattering with that of a reference solution of BSA (MM=66 kDa). The volume of the hydrated particle was computed using the Porod invariant equation (38). The low resolution shape of the molecule was computed *ab initio* using the program DAMMIN (39), which uses an assembly of densely packed beads to represent the protein molecule. Simulated annealing was used to build a compact, interconnected configuration of beads inside a sphere with the diameter D_{max} that fits the experimental data $I_{exp}(s)$ to minimize the discrepancy:

$$\chi^2 = \frac{1}{N-1}\sum_j \left[\frac{I_{exp}(s_j) - cI_{calc}(s_j)}{\sigma(s_j)}\right]^2$$

where N is the number of experimental points, c is a scaling factor and $I_{calc}(s)$, and $\sigma(s_j)$ are the calculated intensity and the experimental error at the momentum transfer s_j, respectively.

The scattering from the crystallographic model of ROCKI (protein fraction of PDB entry 2ETR; 25) was calculated using CRYSOL (40). The model of dimeric DMPKΔCC/VR was constructed based on the structure of ROCKI using the program BUNCH (41). The dimerization domains consisting of the 70 N-terminal and 20 C-terminal residues of ROCKI remained fixed during the calculations, so that the subunit interface stayed unaltered. The kinase domain was allowed to move as a rigid body while the missing C-terminal tail in DMPKΔCC/VR was represented as an interconnected chain of dummy residues (for domain definition, see Fig 6*a*) (42). A simulated annealing protocol was used to position the kinase domain and find the configuration of the C-terminal fragment that could fit the experimental scattering while obeying the P2 symmetry of the dimer.

RESULTS

Crystal structure of DMPK-CC

The structure of DMPK-CC (residues 461–537; Fig. 1) has been elucidated by X-ray crystallography up to 1.6 Å resolution. X-ray data statistics and model refinement parameters are given in **Table 1**. Crystals contain three polypeptide chains in the asymmetric unit, which form a consecutive coil of 86.5 Å length, spanning residues 466–527 and comprising eight complete heptad repeats. They build a parallel, left-handed trimeric motif (**Fig 2*a***).

The architecture of DMPK-CC is restrained at its terminal sections while a central region exhibits moderate structural fluctuations as indicated by crystallographic temperature factors and interchain conformational agreement (Fig 2*a, b*). The relative structural slackness at the middle point of the domain correlates with a widening of the coil at that position (Fig 2*c*), which is likely to be caused by the presence of a sequence motif, 493-IRTD-496, with low propensity for CC formation (estimated using MultiCoil; 43). Also noticeable is a residue located upstream, R483, which contributes a charged group in core position *a* with a reduced Crick-phase (–2.8° instead of the commonly

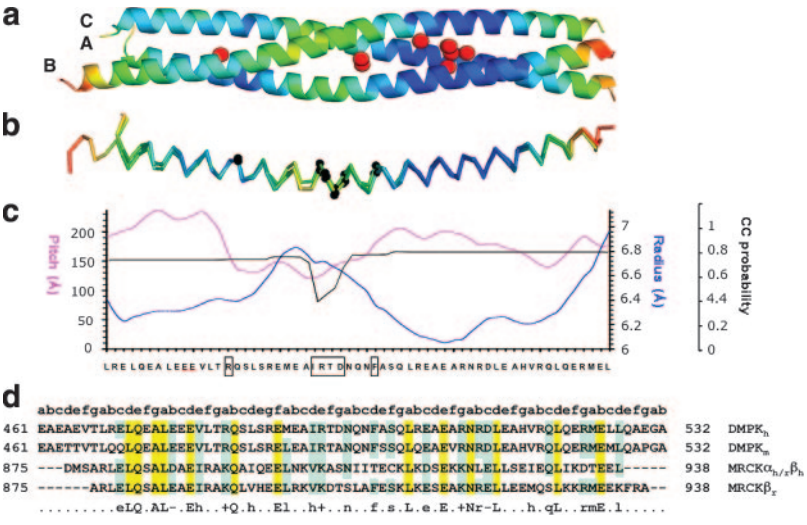

Figure 2. Crystal structure of DMPK-CC. *a)* Ribbon representation colored in a blue-to-red gradient according to crystallographic B-factors (8 to 55 $Å^2$), where blue designates low values. Solvent atoms in the interior of the CC motif are displayed as red spheres; *b)* Superimposition of chains A, B, and C colored as in panel *a*. Cα atoms of residues influencing coil parameters are shown as black spheres; *c)* coil parameter values for pitch, radius and residue tendency to coil formation. Residues leading to coil alterations are boxed; *d)* sequence alignment of DMPK-CC and MRCK-CC3. Identity is shown in yellow and similarity in green.

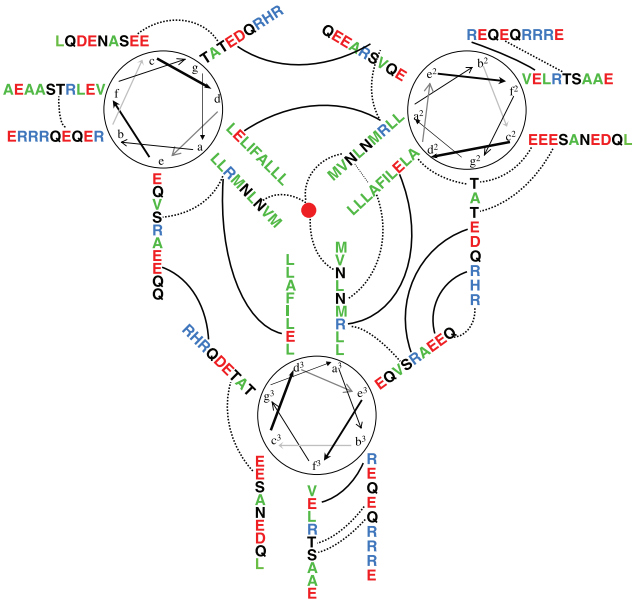

Figure 3. Intra- and interchain interactions in DMPK-CC. Green represents hydrophobic groups, red is negatively charged, blue is positively charged, and black, all other residues. The central red sphere represents an internal solvent atom located at the 3-fold axis and coordinating the three side chains of N511. Interactions are shown as connecting lines, where salt bridges are in black.

encountered value of −40°, as calculated using Twister; 44). This leads to overtwisting of the subsequent coil portion (Fig 2*c*) and an associated suboptimal hydrophobic core packing in that region. Thus, central coil widening and pitch parameters appear not to simply reflect crystal lattice restraints but to be an intrinsic structural feature of this CC domain.

Residue arrangements around the 3-fold axis of DMPK-CC are mostly symmetrical, an exception are the side chains of F500, an aromatic residue in position *d*. The presence of aromatic groups in core positions is extremely rare in dimeric CCs, but it is observed in trimeric motifs (45). For example, the trimeric coil of lung surfactant protein D (46) contains F225 and Y228 in *a* and *d* positions, respectively, which exhibit similar asymmetrical arrangements of their side chains. This is likely to reflect the difficulty of packing bulky groups in the limited interior of a trimeric coil. Remarkably, DMPK-CC also houses several solvent molecules in its core. In particular, its C-terminal section comprises an internal cavity filled by solvent that stabilizes a polar residue, N511, in *a* core position. A similar arrangement has been found in other trimeric CCs, such as bacteriophage T4 fibritin (47) and a domain of a coat protein from MoMuLVirus (48). Such buried polar groups in CCs are thought to contribute to the specificity of the motif and to maintain chain registry (49). Other relevant interactions in DMPK-CC (**Fig. 3**) include 6 interchain and 2 intrachain salt bridges. Interchain bridges help defining the association state of CCs, while intrachain bridges are important for helix stability (50). The interchain bridges of DMPK-CC belong both to the classical types *eg'*RE and *eg'*ER and to unusual core contacts of type *ad'*RE (notation as in ref 40; where ' designate residues in a subsequent heptad repeat). Intrachain salt bridges in DMPK-CC are of type *bf*RE. It is striking that the sequence of DMPK-CC is rich in charged residues (16E, 9R, vs. 2D, 0K per chain), although less than half of these are involved in interactions (8E, 4R, 0D). Thus, availability of reactive groups in the surface of this domain is high (predominantly of a negatively charged character and toward the NH_2 terminus of the domain), so that it could support electrostatic binding to other molecular components.

Characterization of DMPK-CC in solution

In agreement with crystallographic data, the association state of DMPK-CC in solution is trimeric. One single oligomeric species could be detected using native-PAGE, size exclusion chromatography (**Fig 4*a***), and a sedimentation velocity study, which produced a single migrating boundary corresponding to a S_{20W} of 2,1. Thus, the sample population in solution appeared to be highly homogeneous, with no dynamic states of assem-

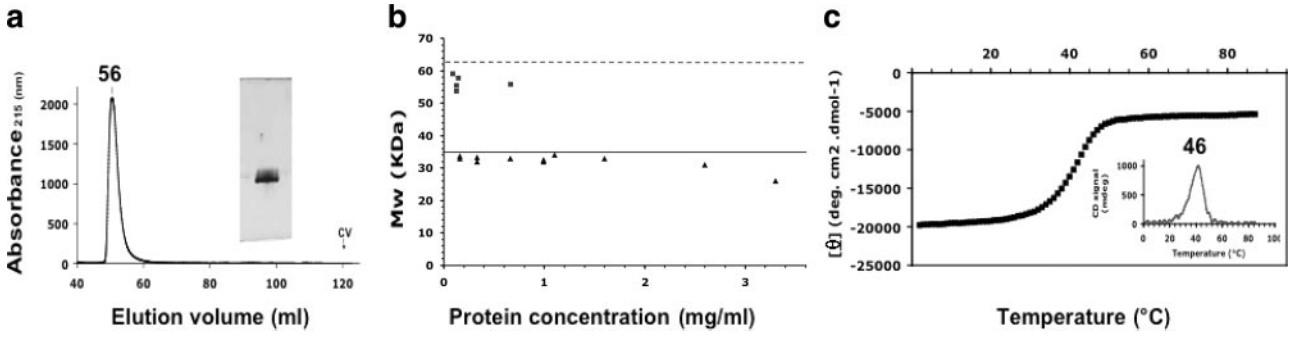

Figure 4. Biophysical characterization of DMPK-CC in solution. *a)* Size exclusion chromatogram in 50 mM Tris-HCl pH 7.5, 100 mM NaCl using a Superdex 75 Hi Load 16/60 column. A native-PAGE is shown in the inset; *b)* molecular mass calculated from sedimentation equilibrium measurements for DMPK-CC (triangles) and DMPK-CC^{N+} (squares). Buffer conditions as in panel *a*. Theoretical mass values for trimeric formations are indicated by horizontal bars, where a continuous line corresponds to DMPK-CC and a dashed line to DMPK CC^{N+}. *c)* Thermal denaturation curve monitored by circular dichroism. First derivative is shown.

bly being observed. Sedimentation equilibrium analysis of DMPK-CC yielded an average molecular mass (MM) of ~33 kDa over the entire protein concentration range assayed (0.16–3.3 mg/ml), consistent with the single presence of trimers in the solutions (theoretical MM for a trimer of this construct 34.9 kDa; Fig 4*b*). Since the sample remained fully assembled at the lowest concentration assayed, the Kd of the interaction must be lower than 4 μM.

These studies carried out at moderate ionic strength (50–100 mM NaCl) and limited protein concentration are in good agreement with crystallographic data obtained from high salt solutions (2.0 M Na^+/K^+ tartrate) or polyethylene glycol media and concentrated protein samples (5–10 mg/ml), both at pH 4.6 and 7.5 (28). This suggests that the trimeric formations of DMPK-CC are stable in a broad range of media conditions. To gain further insight into the stability of this domain, it was investigated by thermal denaturation monitored by circular dichroism. A monophasic melting curve was recorded characteristic of a cooperative helix-coil transition of the three chains as a single domain, with a $T_{1/2m}$ of 46°C (Fig 4*c*). This measurement was carried out in 100 mM sodium phosphate buffer pH 7.0, 100 mM NaCl at a protein concentration of 0.6 mg/ml. To account for specific buffer effects, measurements were repeated in 50 mM bis-Tris propane pH 7.5, 100 mM NaCl with equivalent results. This indicates a strong association of the component chains and confirms the robustness of the assembly. Therefore, it can be concluded that DMPK-CC has a strong tendency to self-associate into well-defined trimeric formations.

Oligomeric state of DMPK variants containing and lacking the CC domain

The assembly level of a DMPK construct comprising the LR sequence, the kinase domain, and the CC fraction, DMPKΔVR (Fig. 1), was investigated using multiangle light scattering coupled to size exclusion chromatography (SEC-MALS). This construct closely resembles an expressed DMPK spliceoform and is a suitable representative of this kinase in the cell. The study yielded MMs of 122′7 kDa and 124′5 kDa for protein concentrations estimated using UV-A_{280} and refractive index, respectively. These values are in excellent agreement with the calculated MM of 120′2 kDa for a dimer of this sample (**Fig. 5**). This result is consistent with previous sedimentation equilibrium data on a comparable construct of this kinase (23).

To investigate the contribution of DMPK-CC to the dimerization of this kinase, a truncated variant lacking the CC fraction, DMPKΔCC/VR (Fig. 1), was examined. Data from size exclusion chromatography and native PAGE indicated the presence of a single species of DMPKΔCC/VR in solution, and SEC-MALS measurements confirmed that this corresponded to dimeric formations (Fig. 5). The experimental MM estimated for this sample was 101′4 kDa and 107′4 kDa using

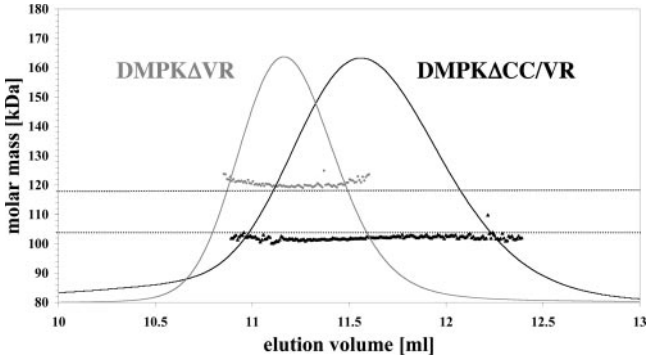

Figure 5. SEC-MALS characterization of DMPKΔVR and DMPKΔCC/VR. Molar mass (dots) and normalized UV signals are shown. The theoretical molar masses of the dimers of DMPKΔVR and DMPKΔVR/CC (120.0 kDa and 106.6 kDa, respectively) are indicated with horizontal lines.

UV-A_{280} and refractive index to estimate the protein concentration, respectively. This is in close agreement with the theoretical MM of 106′6 kDa for a dimer of this construct. Furthermore, samples remained monodisperse and data were consistent through injected protein concentrations of 0.3–2 mg/ml, indicating that results are concentration independent (data not shown). The assembly state of DMPKΔVR coincides with that of DMPKΔCC/VR but not DMPK-CC, showing that the association level of this kinase is not dictated by the oligomerization properties of its CC domain and that segments associated with the kinase domain bear this function instead.

Analysis of DMPKΔCC/VR dimers by small angle X-ray scattering

The kinase domain of DMPK is flanked by an N-terminal region of ~65 residue length (LR) and a C-terminal tail containing ~120-residues that links it to the CC domain (Fig. 1). Recent crystallographic data on ROCKI (25) show that, in that kinase, sequences both N- and C-terminal to the kinase domain pack together to form a dimerization domain. It has been shown that the single presence of the α-helical LR region is not sufficient to secure assembly in this case, so that the removal of the kinase C-terminal tail results in ~80% monomeric species (24). Given that ROCKI and DMPK share homology in the mentioned regions (22% and 36% seq. id. in the LR domain and kinase tail, respectively; **Fig 6*a***), we investigated whether DMPK might follow the same architectural principles of ROCKI by analyzing the overall conformation of DMPKΔCC/VR dimers using SAXS.

The experimental SAXS pattern of DMPKΔCC/VR is displayed in Fig 6*b*. The estimated MM, 95 ± 10 kDa, confirms that the protein is dimeric under the SAXS experimental conditions. This is further corroborated by the volume of the hydrated particle, 210 ± 10 × 10^3Å (3), noting that, for globular proteins, the hydrated volume in $Å^3$ should be approximately twice the MM in daltons. The radius of gyration R_g and the maximum particle size D_{max} were 39.9 ± 0.6 Å and

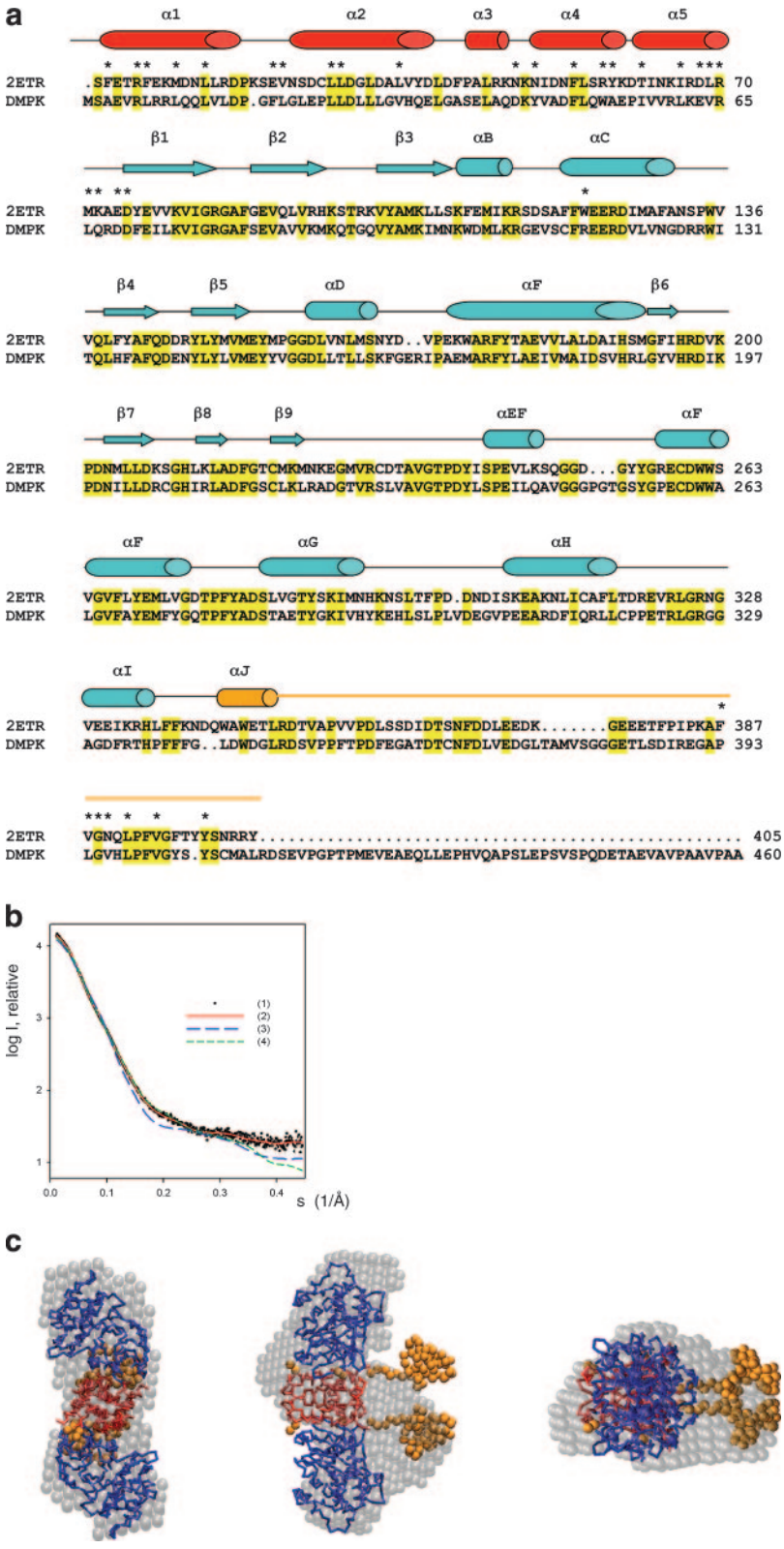

Figure 6. SAXS analysis of DMPKΔCC/VR dimers (*a*). Sequence similarity between DMPKΔCC/VR and the crystallographic model of ROCKI (PDB code 2ETR). Sequence identity is highlighted in yellow. Secondary structure elements are as in ref 25. Domain definition is as follows: red corresponds to the LR domain, blue to the kinase domain, and golden to the C-terminal tail. ROCKI residues involved in dimerization are marked with an asterisk. *b)* Experimental scattering of DMPKΔCC/VR (1) and calculated patterns from the *ab initio* low-resolution bead model (2), the ROCKI crystallographic model (3) and the reconstructed DMPKΔCC/VR model with an added C-terminal fraction (4); *c) ab initio* model of DMPKΔCC/VR (gray semitransparent beads) superimposed on the model constructed by adding C-terminal particles (orange beads) to the protomers of ROCKI (Cα-trace). Domain coloring as in *a*. Three orthogonal views are shown.

130 ± 10 Å, respectively, suggesting an elongated structure. This agrees with the low-resolution shape of DMPKΔCC/VR reconstructed *ab initio*, which fits neatly the experimental data with a discrepancy $\chi = 0.95$ (Fig 6*b*). A comparison of this with the crystal structure of ROCKI indicates that DMPKΔCC/VR has a similar overall conformation, also appearing to form head-to-head dimers (Fig 6*c*). The low-resolution model of DMPKΔCC/VR, however, displayed extra electron density that was not satisfied by the ROCKI structure, as can be expected from the fact that each protomer of DMPKΔCC/VR has 65 additional residues at its C terminus (Fig 6*a*). The missing residues account for 14% of the total scattering mass of this sample. They

play a significant role in the scattering of this molecule, possibly due to their contribution to an anisometric molecular shape (see below), so that the patterns computed from ROCKI yielded a poor fit to the experimental data (χ=6.6; Fig 6*b*). To construct a model of DMPKΔCC/VR, the missing C-terminal portion was generated for each monomer using beads and maintaining a 2-fold symmetry as described in Materials and Methods. Although during the calculation the kinase domain was allowed to drift and rotate as a rigid body, its position was practically unchanged with respect to ROCKI. Models of DMPKΔCC/VR so generated showed that the C-terminal portions of each protomer formed rather compact formations, suggesting the existence of a protein domain at this position. A typical model of DMPKΔCC/VR in solution provides a good fit to the experimental data (χ=1.75; Fig 6*b*) and agrees well with the molecular shape calculated *ab initio* as revealed by a comparative superimposition (Fig 6*c*). A deviation between models, however, shows that the volumes occupied by the C-terminal fraction are represented somewhat differently by the two modeling methods. It should be noted that the *ab initio* model was obtained without imposing any prior knowledge or symmetry restrictions, whereas the reconstructed model applies a 2-fold symmetry that may not be entirely adhered to by a potentially flexible C-terminal tail. Such flexibility could underlie localized deviations between otherwise consistent models and scattering patterns.

CC domains can be found in proteins in combination with other motifs that influence their association. The most prominent example is that of the trimeric CC of fibritin, which is followed by a C-terminal extension of ~30 residue length that folds into a β-hairpin (51). This intertwines with equivalent β-hairpins from other subunits, being essential to achieve CC trimerization in that case. Given that SAXS models of DMPKΔCC/VR suggested the presence of a structural formation immediately prior to the CC fraction, we assayed whether this might act as an association motif that could modulate CC stoichiometry. For this, we constructed an N-terminally extended version of DMPK-CC, DMPK-CC^{N+} (Fig. 1), and analyzed its oligomeric state by sedimentation equilibrium (Fig 4*b*). Results indicated that DMPK-CC^{N+} remained trimeric (estimated MM 56.1 kDa compared to a theoretical MM of 63.5 kDa for a trimer of this construct), suggesting that possible structural elements of the kinase-CC linker sequence do not influence the oligomerization of this coil.

DMPK-CC is not involved in domain interactions

The CC fractions of ROCKs and MRCK have been shown to interact directly with their respective kinase domains, thereby acting as intrasteric inhibitors of kinase activity (26, 27). In ROCKs, the interaction involves the Rho binding site at the C terminus of its long CC domain, whereas in MRCK the binding has been mapped to a fragment spanning CC2/CC3, whose deletion resulted in about a 3-fold increase in activity. Given that DMPK-CC and MRCK-CC3 share certain sequence similarity (up to 31% identity according to isoforms) (Fig 2*d*), we investigated the possible interaction of DMPK-CC with other domains in this kinase using pull-down assays as well as coexpression/copurification experiments on DMPK-CC and DMPKΔCC/VR. Binding between these species could not be detected by either procedure, which yielded independent original species. Hence, DMPK-CC appears to neither interact with the kinase domain nor form a hetero-coil against the α-helical LR sequence. This indicates that a CC association/dissociation regulatory model such as that proposed for MRCK and ROCKs is unlikely to be applicable to DMPK and that the kinase and CC fractions component of DMPK are likely to be arranged as architecturally distinct fractions, resulting in a globular portion and a filamentous shaft.

DISCUSSION

The CC domains of DMPK-related kinases are essential to the regulation of their catalytic activities. However, the molecular events mediated by these domains are yet to be accurately understood. CC sequences in this family exhibit large variability in length and composition, sharing little or no similarity. Only minimal structural data exist that aid to clarify the respective properties and functional roles of CC domains within this family. Here we report the crystal structure of DMPK-CC, which is unrelated to the ROCKs-CCs previously described (21, 22). Contrary to the dimeric character of the latter fragments, DMPK-CC forms a trimeric motif that is characterized by rigid termini and a central widening of its coil. It is currently unknown whether this feature might reflect functional properties of this domain. As proven by sedimentation equilibrium data, the assembly level of DMPK-CC in solution coincides with that in the crystal. No other oligomeric state has been detected in the current study under a broad range of protein concentration and ionic strength conditions. Furthermore, thermal denaturation studies have shown this assembly to be stable. Thus, our data prove that the oligomeric states of CC domains from this kinase family are more diversified than previously expected and that more coils must be investigated before general conclusions on their self-association properties can be drawn.

Experimental results on DMPK-CC contrast markedly with sequence-based predictions, which suggests this coil forms dimeric assemblies. For example, the software MultiCoil (43) estimates 82% probability of dimer vs. 10% trimer formation. The structural determinants of CC association remain poorly understood, and thus such predictions should be considered with caution. Only a few systematic analyses have addressed the basis of CC association experimentally, focusing on either the role of hydrophobic core residues (52, 53) or salt bridges (e.g., 54, 55). Consequently, cases are described where experimental data disagree with predictions (for

example, see ref 46). To understand the molecular basis of DMPK-CC trimerization, we analyzed its interchain contacts. The only factor that might be proposed at this time to favor formation of trimers over dimers is the presence of an aromatic residue, F500, at core position *a*, since this is rarely observed in dimeric coils (45). The contribution of the several salt bridges in DMPK-CC to its oligomerization cannot be evaluated based on current knowledge.

Given that CCs are established oligomerization motifs, these were initially thought to be indispensable for the molecular assembly of DMPK-related kinases. However, recent studies of ROCKs have shown that other domains mediate self-association in these kinases, namely, the N-terminal LR region and a tail C-terminal to the kinase domain (24, 25). Similarly, in the current study, a truncated DMPK variant lacking the CC moiety formed dimeric assemblies according to SEC-MALS data. A low-resolution structural analysis of these dimers using SAXS indicated that DMPK and ROCKI share similar dimerization principles involving head-to-head protomer interactions, even though a certain number of residues involved in the dimerization of ROCKI are not conserved in DMPK (Fig 6*a*). Our data on the truncated DMPK variant differ from those of a previous study (23), where a similar DMPK construct was argued to be monomeric according to sucrose density gradient sedimentation and pull-down assays. The dimeric form in our study (residues 1–460) contains 29 more residues at its C terminus than the construct previously reported. The truncation in that case might have disrupted a possible structural element C-terminal to the kinase domain, which has been insinuated by current SAXS data. More studies are required to identify the exact structural details of this segment of DMPK and to establish whether its integrity is essential for the assembly of this kinase. Contrary to that former study, we conclude that the CC domain of DMPK is not required for its self-association and that a common architectural design is likely to be shared by the closest members of this family: DMPK, MRCK, and ROCKs.

The fact that an interaction between DMPK-CC and other domains in DMPK could not be identified in the current study suggests it is unlikely that the assembly properties of this CC are altered by a possible embedding within the kinase core. Neither is the influence of flanking structural elements expected, given that an N-terminally extended CC construct retained the same oligomerization concentration. Thus, we speculate that the stoichiometry of this coil within the context of full DMPK must be dominated by the prior association of the N-terminal catalytic fraction into dimers. Prediction data confirm that the DMPK-CC sequence is geometrically compatible with a dimeric association, and it is known that CC oligomerization can be dynamically altered by local factors (20).

Oligomerization is crucial for the activation of numerous kinases. Often self-assembly is directed to ensure efficient autophosphorylation in *trans* by increasing the local concentration of catalytic domains (56). Given that DMPK-CC does not determine the self-association of this kinase and that, contrary to MRCK and ROCKs, it does not act as an intrasteric inhibitor but as an activator, further investigations are needed to clarify whether its function might relate instead to the achievement of an active conformation or even substrate docking. Moreover, given the heterogeneity in CC sequences and their diversified interaction patterns across DMPK-related kinases, studies are required to reveal the exact role of these moieties and to establish the principles of their regulatory mechanisms. FJ

Thanks go to Prof. B. Perryman for facilitating the initial DNA coding for DMPK. A special mention goes to R. Ravelli at ID14–2 (ESRF) for exceptional assistance during data collection. Thanks go to S. Strelkov for critical reading of this manuscript. Most sincere gratitude goes to Prof. A. Plückthun for generous support with SEC-MALS. We acknowledge the support of Swiss National Foundation (grant 3100A0–100852) and to P.G. of Association Française contre les Myopathies (grant 9812).

REFERENCES

1. Fu, Y. H., Pizzuti, A., Fenwick, R. G., Jr., King, J., Rajnarayan, S., Dunne, P. W., Dubel, J., Nasser, G. A., Ashizawa, T., de Jong, P., et al. (1992) An unstable triplet repeat in a gene related to myotonic muscular dystrophy. *Science* **255**, 1256–1258
2. Brook, J. D., McCurrach, M. E., Harley, H. G., Buckler, A. J., Church, D., Aburatani, H., Hunter, K., Stanton, V. P., Thirion, J. P., Hudson, T., et al. (1992) Molecular basis of myotonic dystrophy: expansion of a trinucleotide (CTG) repeat at the 3′ end of a transcript encoding a protein kinase family member. *Cell* **68**, 799–808
3. Nakagawa, O., Fujisawa, K., Ishizaki, T., Saito, Y., Nakao, K., and Narumiya, S. (1996) ROCK-I and ROCK-II, two isoforms of Rho-associated coiled-coil forming protein serine/threonine kinase in mice. *FEBS Lett.* **392,** 189–193
4. Ishizaki, T., Maekawa, M., Fujisawa, K., Okawa, K., Iwamatsu, A., Fujita, A., Watanabe, N., Saito, Y., Kakizuka, A., Morii, N., and Narumiya, S. (1996) The small GTP-binding protein Rho binds to and activates a 160 kDa Ser/Thr protein kinase homologous to myotonic dystrophy kinase. *EMBO J.* **15,** 1885–1893
5. Wissmann, A., Ingles, J., McGhee, J. D., and Mains, P. E. (1997) Caenorhabditis elegans LET-502 is related to Rho-binding kinases and human myotonic dystrophy kinase and interacts genetically with a homolog of the regulatory subunit of smooth muscle myosin phosphatase to affect cell shape. *Genes Dev.* **11,** 409–422
6. Luo, L., Lee, T., Tsai, L., Tang, G., Jan, L. Y., and Jan, Y. N. (1997) Genghis Khan (Gek) as a putative effector for Drosophila Cdc42 and regulator of actin polymerization. *Proc. Natl. Acad. Sci. USA* **94,** 12963–12968
7. Di Cunto, F., Calautti, E., Hsiao, J., Ong, L., Topley, G., Turco, E., and Dotto, G. P. (1998) Citron rho-interacting kinase, a novel tissue-specific ser/thr kinase encompassing the Rho-Rac-binding protein Citron. *J. Biol. Chem.* **273,** 29706–29711
8. Leung, T., Chen, X. Q., Tan, I., Manser, E., and Lim, L. (1998) Myotonic dystrophy kinase-related Cdc42-binding kinase acts as a Cdc42 effector in promoting cytoskeletal reorganization. *Mol. Cell. Biol.* **18,** 130–140
9. Madaule, P., Eda, M., Watanabe, N., Fujisawa, K., Matsuoka, T., Bito, H., Ishizaki, T., and Narumiya, S. (1998) Role of citron kinase as a target of the small GTPase Rho in cytokinesis. *Nature* **394,** 491–494
10. Piekny, A. J., and Mains, P. E. (2002) Rho-binding kinase (LET-502) and myosin phosphatase (MEL-11) regulate cytokinesis in the early *Caenorhabditis elegans* embryo. *J. Cell Sci.* **115,** 2271–2282
11. Kosako, H., Yoshida, T., Matsumura, F., Ishizaki, T., Narumiya, S., and Inagaki, M. (2000) Rho-kinase/ROCK is involved in cytokinesis through the phosphorylation of myosin light chain

and not ezrin/radixin/moesin proteins at the cleavage furrow. *Oncogene* **19,** 6059–6064
12. Jin, S., Shimizu, M., Balasubramanyam, A., and Epstein, H. F. (2000) Myotonic dystrophy protein kinase (DMPK) induces actin cytoskeletal reorganization and apoptotic-like blebbing in lens cells. *Cell Motil. Cytoskeleton* **45,** 133–148
13. Schulz, P. E., McIntosh, A. D., Kasten, M. R., Wieringa, B., and Epstein, H. F. (2003) A role for myotonic dystrophy protein kinase in synaptic plasticity. *J. Neurophysiol.* **89,** 1177–1186
14. Shimizu, M., Wang, W., Walch, E. T., Dunne, P. W., and Epstein, H. F. (2000) Rac-1 and Raf-1 kinases, components of distinct signaling pathways, activate myotonic dystrophy protein kinase. *FEBS Lett.* **475,** 273–277
15. Mounsey, J. P., Mistry, D. J., Ai, C. W., Reddy, S., and Moorman, J. R. (2000) Skeletal muscle sodium channel gating in mice deficient in myotonic dystrophy protein kinase. *Hum. Mol. Genet.* **9,** 2313–2320
16. Lee, H. C., Patel, M. K., Mistry, D. J., Wang, Q., Reddy, S., Moorman, J. R., and Mounsey, J. P. (2003) Abnormal Na channel gating in murine cardiac myocytes deficient in myotonic dystrophy protein kinase. *Physiol. Genomics* **12,** 147–157
17. Harper, P. S. (1989) *Myotonic Dsytrophy,* Saunders, London/Philadelphia
18. Davis, B. M., McCurrach, M. E., Taneja, K. L., Singer, R. H., and Housman, D. E. (1997) Expansion of a CUG trinucleotide repeat in the 3′ untranslated region of myotonic dystrophy protein kinase transcripts results in nuclear retention of transcripts. *Proc. Natl. Acad. Sci. USA* **94,** 7388–7393
19. Jiang, H., Mankodi, A., Swanson, M. S., Moxley, R. T., and Thornton, C. A. (2004) Myotonic dystrophy type 1 is associated with nuclear foci of mutant RNA, sequestration of muscleblind proteins and deregulated alternative splicing in neurons. *Hum. Mol. Genet.* **13,** 3079–3088
20. Lupas, A. N., and Gruber, M. (2005) The structure of alpha-helical coiled coils. *Adv. Protein Chem.* **70,** 37–78
21. Shimizu, T., Ihara, K., Maesaki, R., Amano, M., Kaibuchi, K., and Hakoshima, T. (2003) Parallel coiled-coil association of the RhoA-binding domain in Rho-kinase. *J. Biol. Chem.* **278,** 46046–46051
22. Dvorsky, R., Blumenstein, L., Vetter, I. R., and Ahmadian, M. R. (2004) Structural insights into the interaction of ROCKI with the switch regions of RhoA. *J. Biol. Chem.* **279,** 7098–7104
23. Zhang, R., and Epstein, H. F. (2003) Homodimerization through coiled-coil regions enhances activity of the myotonic dystrophy protein kinase. *FEBS Lett.* **546,** 281–287
24. Doran, J. D., Liu, X., Taslimi, P., Saadat, A., and Fox, T. (2004) New insights into the structure-function relationships of Rho-associated kinase: a thermodynamic and hydrodynamic study of the dimer-to-monomer transition and its kinetic implications. *Biochem. J.* **384,** 255–262
25. Jacobs, M. D., Hayakawa, K., Swenson, L., Bellon, S. F., Fleming, M., Taslimi, P., and Doran, J. (2005) The structure of dimeric rock 1 reveals the mechanism for ligand selectivity. *J. Biol. Chem.* Oct 24; [Epub ahead of print]
26. Tan, I., Seow, K. T., Lim, L., and Leung, T. (2001) Intermolecular and intramolecular interactions regulate catalytic activity of myotonic dystrophy kinase-related Cdc42-binding kinase alpha. *Mol. Cell. Biol.* **21,** 2767–2778
27. Amano, M., Chihara, K., Nakamura, N., Kaneko, T., Matsuura, Y., and Kaibuchi, K. (1999) The COOH terminus of Rho-kinase negatively regulates rho-kinase activity. *J. Biol. Chem.* **274**, 32418–32424
28. Garcia, P., Marino, M., and Mayans, O. (2004) Crystallization and preliminary X-ray analysis of the coiled-coil domain of dystrophia myotonica kinase. *Acta Crystallogr. D* **60,** 2336–2339
29. La Fortelle, E., and Bricogne, G. (1997) *Methods Enzymol.* **276,** 472–494
30. Perrakis, A., Morris, R., and Lamzin, V. S. (1999) Automated protein model building combined with iterative structure refinement. *Nat. Struct. Biol.* **6,** 458–463
31. Jones, T.A, Zou, J.Y., Cowan, S. W., and Kjeldgaard, M. (1991) Improved methods for building protein models in electron density maps and the location of errors in these models. *Acta Crystallogr. A* **47,** 110–119
32. Murshudov, G. N., Vagin A.A., and Dodson, E. J. (1997) Refinement of macromolecular structures by the maximum-likelihood method. *Acta Crystallogr D* **53,** 240–255
33. Collaborative Computational Project, N. 4 (1994) *Acta Crystallogr. D* **50,** 760–763
34. Laskowski, R. A., MacArthur, M. W., Moss, D. S., and Thornton, J. M. (1993) PROCHECK: a program to check the stereochemical quality of protein structures. *J. Appl. Crystallogr.* **26,** 283–291
35. Koch, M. H. J., and Bordas, J. (1983) X-ray diffraction and scattering on disordered systems using synchrotron radiation. *Nucl. Instrum. Methods* **208,** 461–469
36. Konarev, P.V., Volkov, V.V., Sokolova, A.V., Koch, M. H. J., and Svergun, D. I. (2003) PRIMUSā Windows-PC based system for small-angle scattering data analysis. *J. Appl. Crystallogr.* **36,** 1277–1282
37. Svergun, D. I. (1992) Determination of the regularization parameter in indirect transform methods using perceptual criteria. *J. Appl. Crystallogr.* **25,** 495–503
38. Porod, G. (1982) Small angle X-ray scattering. (Glatter, O., and Kratky, O., eds) Academic Press, London
39. Svergun, D. I. (1999) Restoring low resolution structure of biological macromolecules from solution scattering using simulated annealing. *Biophys. J.* **76,** 2879–2886
40. Svergun, D. I., Barberato, C., and Koch, M. H. J. (1995) CRYSOLā program to evaluate X-ray solution scattering of biological macromolecules from atomic coordinates. *J. Appl. Crystallogr.* **28,** 768–773
41. Petoukhov, M. V., and Svergun, D. I. (2005) Global rigid body modelling of macromolecular complexes against small-angle scattering data. *Biophys. J.* **89,** 1237–1250
42. Petoukhov, M. V., Eady, N.A., Brown, K. A., and Svergun, D. I. (2002) Addition of missing loops and domains to protein models by x-ray solution scattering. *Biophys. J.* **83,** 3113–3125
43. Wolf, E., Kim, P. S., and Berger, B. (1997) MultiCoil: a program for predicting two- and three-stranded coiled coils. *Protein Sci.* **6,** 1179–1189
44. Strelkov, S. V., and Burkhard, P. (2002) Analysis of alpha-helical coiled coils with the program TWISTER reveals a structural mechanism for stutter compensation. *J. Struct. Biol.* **137,** 54–64
45. Walshaw, J., and Woolfson, D. N. (2001) Socket: a program for identifying and analysing coiled-coil motifs within protein structures. *J. Mol. Biol.* **307,** 1427–1450
46. Hakansson, K., Lim, N. K., Hoppe, H. J., and Reid, K. B. (1999) Crystal structure of the trimeric alpha-helical coiled-coil and the three lectin domains of human lung surfactant protein D. *Structure Fold Des.* **7,** 255–264
47. Tao, Y., Strelkov, S. V., Mesyanzhinov, V. V., and Rossmann, M. G. (1997) Structure of bacteriophage T4 fibritin: a segmented coiled coil and the role of the C-terminal domain. *Structure* **5,** 789–798
48. Fass, D., Harrison, S. C., and Kim, P. S. (1996) Retrovirus envelope domain at 1.7 Å resolution. *Nat. Struct. Biol.* **3,** 465–469
49. Lumb, K. J., and Kim, P. S. (1998) A buried polar interaction imparts structural uniqueness in a designed heterodimeric coiled coil. *Biochemistry* **34,** 8642–8648
50. Burkhard, P., Ivaninskii, S., and Lustig, A. (2002) Improving coiled-coil stability by optimizing ionic interactions. *J. Mol. Biol.* **318,** 901–910
51. Tao Y, Strelkov, S.V., Mesyanzhinov, V.V., and Rossmann, M. G. (1997) Structure of bacteriophage T4 fibritin: a segmented coiled coil and the role of the C-terminal domain. *Structure* **5,** 789–798
52. Harbury, P. B., Zhang, T., Kim, P. S., and Alber, T. (1993) A switch between two-, three-, and four-stranded coiled coils in GCN4 leucine zipper mutants. *Science* **262,** 1401–1407
53. Gonzalez, L., Jr., Woolfson, D. N., and Alber, T. (1996) Buried polar residues and structural specificity in the GCN4 leucine zipper. *Nat. Struct. Biol.* **3,** 1011–1018
54. Kammerer, R. A., Jaravine, V. A., Frank, S., Schulthess, T., Landwehr, R., Lustig, A., Garcia-Echeverria, C., Alexandrescu, A. T., Engel, J., and Steinmetz, M. O. (2001) An intrahelical salt bridge within the trigger site stabilizes the GCN4 leucine zipper. *J. Biol. Chem.* **276,** 13685–13688
55. Meier, M., Lustig, A., Aebi, U., and Burkhard, P. (2002) Removing an interhelical salt bridge abolishes coiled-coil formation in a de novo designed peptide. *J. Struct. Biol.* **137,** 65–72
56. Hubbard, S. R., and Till, J. H. (2000) Protein tyrosine kinase structure and function. *Annu. Rev. Biochem.* **69,** 373–398

Received for publication December 3, 2005.
Accepted for publication February 3, 2006.